Technique for measuring the reflectance of irregular, submillimeter-sized samples

Christopher C. Homes, M. Reedyk, D. A. Cradles, and T. Timusk

Details are given of a technique for measuring the reflectance at near-normal incidence of small, irregular, submillimeter-sized samples from the far IR (40 cm^{-1}) to the visible (40000 cm^{-1}) between 10 and 300 K by using a modified Michelson interferometer or grating spectrometer. The sample and a reference mirror are mounted on nonreflecting cones. At the focus the size of the beam is larger than either the sample or the reference, so that the entire area of the sample is utilized. The positions are interchanged by a 90° rotation by using preset mechanical stops. The scattering caused by geometrical effects is corrected for by the *in situ* evaporation of gold or aluminum onto the sample. The effect of diffraction is estimated from Mie theory by assuming the sample and reference to be spheres. For frequencies above ≈ 40 cm^{-1} and sample diameters of ≈ 1 mm with a detector field of view of 30°, the calculations show that the ratio of the backscattered intensities gives a good approximation of the specular reflectance.

1. Introduction

The most popular method used to find the optical constants of materials that are opaque is the measurement of specular reflectance over a wide range of frequencies followed by a Kramers–Kronig analysis that yields the phase.[1] The optical constants can then be easily calculated. In the field of materials' research often the newest and most interesting materials, such as single crystals of the new high-temperature superconductors, are also the smallest. The samples are frequently irregular in shape, being either polycrystalline with rough granular surfaces or single crystals with cleavage steps lacking large, planar faces. The reflectance technique becomes particularly difficult in the far IR (≤ 200 cm^{-1}) because of the weakness of mercury-arc lamps and the lack of photoconductive detectors.

To compensate for the rough surface, a number of groups have coated the sample surface with a good metal (typically gold) and used the coated sample as reference in the reflectance measurement. If this procedure is performed carefully, much of the structure, because of the interference of rays that reach the detector by different paths and that appear when a flat mirror is used as a reference, is divided out. Figure 1 illustrates this effect. (This particular case is discussed in more detail below.)

In this paper we report on the details of such a method of overcoating. The reflectance is measured at near-normal incidence, and the entire sample area is used (thus permitting small samples to be examined). The scattering effects caused by the surface microstructure are corrected for by using the sample as its own reference by evaporating onto it *in situ* a material whose reflectance is known, such as gold or aluminum.[2] It is assumed that the overcoating is thin enough that it does not change the microstructure of the sample (yet thick enough that it is greater than the penetration depth), so that the ratio of the sample reflectance with respect to the overcoated sample, when multiplied by the reflectance of the coating material, yields a good approximation of the true reflectance of the sample, as it would in the case of specular reflectance. While this technique works particularly well with small samples with irregular surfaces, it is also an excellent way to measure the reflectance of a small sample with a flat surface.

The technique used here permits the entire sample to be illuminated. In the case of a small, specular surface it is impossible to match perfectly the sizes of the sample and reference, so that the reflectance cannot be measured directly. If the surface is irregular, this problem is even more complicated, and the ratios measured with a flat reference mirror can be used only to calculate the reflectance if the sample is overcoated and used as a final reference.

A potential problem with the method is the implicit

The authors are with the Department of Physics and Astronomy, McMaster University, Hamilton, Ontario L8S 4M1, Canada.

Received 21 April 1992.
0003-6935/93/162976-08$06.00/0.

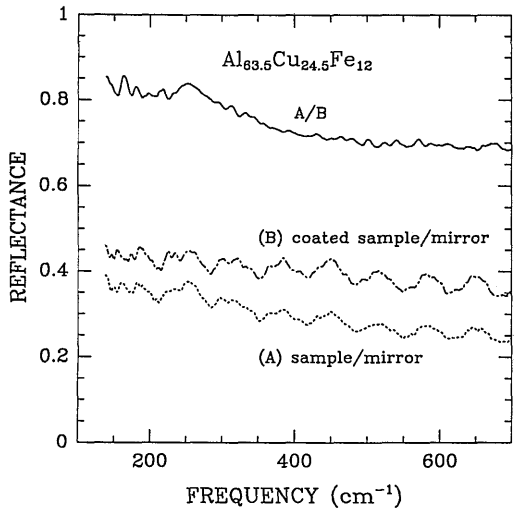

Fig. 1. Reflectance determined by the *in situ* evaporation technique for $Al_{63.5}Cu_{24.5}Fe_{12}$ at room temperature. The short-dashed curve shows the ratio of the sample with respect to a polished stainless-steel reference mirror (A), and the dot–dashed curve shows the same ratio after a thin layer of gold has been evaporated onto the sample (B). The ratio of the two curves, A/B, is shown by the solid curve. This curve is the reflectance of $Al_{63.5}Cu_{24.5}Fe_{12}$ with respect to gold. Note that all of the fine structure in (A) and (B) has been eliminated.

assumption that the diffraction effects for wavelengths comparable with the sample size and with the size of the irregularities of the surface will cancel out in the overcoating process. While the experimental data seem to bear this out, it is difficult to justify this theoretically. To estimate the effect of diffraction from samples of the same size, but with different optical properties, we performed a model calculation using Mie theory, assuming that both the sample and reference were spheres (see Appendix A). The calculations for the spheres show that the diffraction effects appear as oscillations when the sphere is compared with a specular reflector but that the overcoating process reduces the amplitude of the oscillations. Furthermore, despite the presence of fringes, the average value of the calculated reflectance by the overcoating method is a close approximation to the specular reflectance of the sample material.

This method has a number of advantages over other techniques used to measure the reflectance of small crystals. One such technique is to assemble mosaics composed of many small crystals.[3,4] A mosaic can introduce a number of problems, such as the effect of the signal from the epoxy used to assemble the individual crystals. Other techniques are designed for small, single crystals, but they often require that the signal from the sample and the reference be remaximized each time they are interchanged, leading to errors in the absolute value of the reflectance.[5] Also, this latter technique can use only high-quality crystals. In both of the previous cases the size of the aperture at the focus must be smaller than the crystal, so that only a portion of the crystal is actually used, whereas the method presented here uses the entire surface of the sample.

2. Experiment

A. Optical Layout

The optical layout of the reflectance module is shown in Fig. 2. The same optical (and cryogenic) setup may be used with either a grating spectrometer (in the visible regions) or an interferometer (for the far IR). However, because the technique is identical in both cases and because the significance of this technique lies in its application to interferometers, only the latter case is discussed in detail.

The chamber begins at the intermediate focus of a Beckman/RIIC FS 720 Fourier-transform interferometer, modified for a scanning mirror. A vibrating blade chopper used during alignment A sits just before an adjustable circular aperture B, which is located at the intermediate focus of the instrument. The beam is redirected by a plane mirror C to an $f/8$ mirror D, which is focused onto the sample (reference) G, with an angle of incidence of $\sim 5°$ off normal. The reflected light is then collected by a large $f/2.5$ toroidal mirror E and focused onto a detector M. Toroidal mirrors that are adequate for this purpose can be ordered from prescription lens makers as cylindrical plano–concave lenses designed to correct astigmatism.

The beam must pass through an optical window to reach the sample. To avoid window reflections, ei-

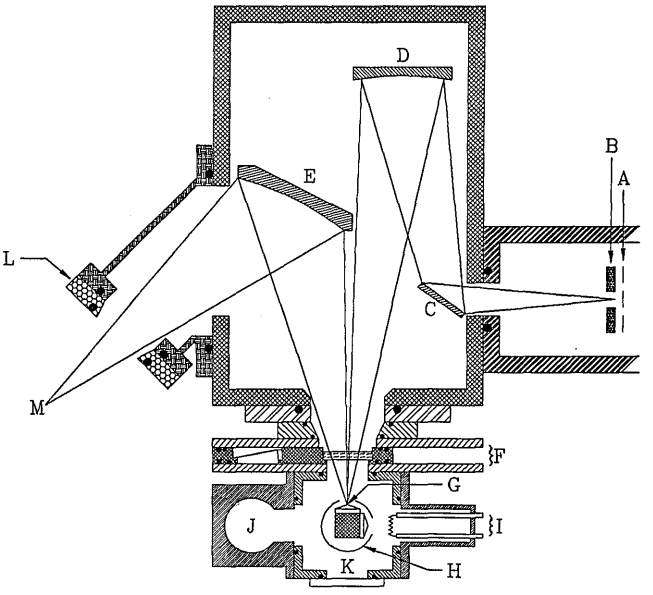

Fig. 2. Horizontal optical arrangement of the reflectance module. The following elements are used: A, vibrating blade chopper; B, adjustable aperture; C, plane mirror; D, $f/8$ toroidal mirror; E, $f/2.5$ toroidal mirror; F, sliding window holder shown with the thick window in position; G, cold tail of cryostat and sample mounts (cones); H, aluminum radiation shield; I, evaporator apparatus; J, ionization tube fitting; K, optical viewing port; L, insulating flange; M, the detector focus. The solid circles represent O-ring seals, and the solid rectangles represent Teflon backup O-rings. (All dimensions are approximate.)

ther the window is angled to reflect light away from the mirror (for thin windows) or a post is inserted to block the reflected light (used for thick windows). The post does not interfere with specular reflection from the sample or reference. With this optical system the magnification of the system is unity. Detectors are electrically isolated from the interferometer by an insulating flange L. The optical components used in the experiments are listed in Table 1. In the far IR either a 1.2-K or 4.2-K silicon bolometer is used. In the mid-IR 4.2-K Si:B and 77-K HgCdTe photoconductive detectors are used.

B. Cryogenic Arrangement

The sample is mounted in an R. G. Hansen High-Tran continuous-flow cryostat, modified to increase the precision of rotation, as shown in Fig. 3, permitting the reflectance to be measured between 10 and 300 K. A collar has been attached to the top of the refrigerator, and it is held in place by a projecting lip as well as by set screws to prevent it from slipping. The High-Tran is thus supported by the collar, which in turn sits on a thrust bearing, permitting the entire arrangement to rotate freely without mechanical contact with the vacuum shroud. Double O-rings on the neck of the High-Tran provide a vacuum seal. The tail of the refrigerator sits in the standard stainless-steel vacuum shroud, which has a total of five access ports. The ports are used for the following purposes: (1) viewing, (2) evaporator access, (3) optical access, (4) ionization gauge, and (5) vacuum line. The vacuum shroud feeds up through an L bracket, which supports the thrust bearing and permits the entire arrangement to be bolted firmly to the side of the interferometer box. It is important to clamp the top of the transfer siphon (where it is inserted into the High-Tran) in place, since any strain placed on the transfer line may produce misalignments in the tail of the cryostat.

The vacuum shroud is evacuated by a water-cooled diffusion pump with a large liquid-nitrogen cold trap. To minimize outgassing, the pumping assembly has been constructed entirely of stainless steel and placed directly beneath the High-Tran unit to minimize the length of the pumping line. The entire system is also baked-out with a heating tape element at ≈ 80 °C for an hour before any temperature-dependent runs are started; this has been found to improve the vacuum substantially. At the present time the best ultimate vacuum at room temperature is $\approx 10^{-5}$ Torr.

Table 1. Optical Elements Used in Each Frequency Range

Range (cm^{-1})	Source	Beam Splitter	Detector
10–250	Mercury lamp	50G Mylar	1.2-K Bolometer
100–800	Cermet[a]	12G Mylar	4.2-K Bolometer
300–1600	Cermet	6G Mylar	4.2-K Si:B
500–2500	Cermet	KBr/Ge	4.2-K Si:B
500–5000	Tungsten	KBr/Ge	77-K HgCdTe
3000–8000	Tungsten	Quartz/Si	77-K HgCdTe

[a]Cermet refers to a ceramic-metal element.

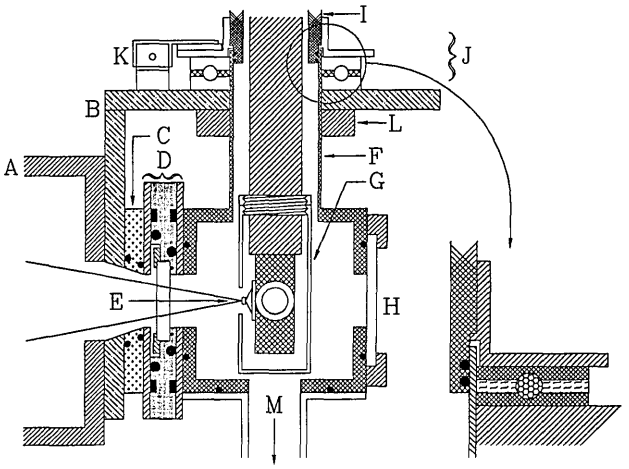

Fig. 3. Vertical arrangement of the cryogenic system. The following elements are shown: A, interferometer box; B, L bracket; C, spacing flange; D, sliding window holder; E, sample and cones on the copper mounting block; F, stainless-steel vacuum shroud; G, aluminum radiation shield and locking washer; H, viewing port; I, High-Tran body; J, thrust bearing and High-Tran support collar; K, mechanical stop; L, locking collar for vacuum shroud; M, 1-in. (2.54-cm) pumping line to the diffusion pump and liquid-nitrogen cold trap. The expanded area shows the collar for the High-Tran and the thrust bearing; note that the collar rotates only on the bearing and does not touch the vacuum shroud. The solid circles indicate O-ring seals, and the solid rectangles represent Teflon backup O-rings. (All dimensions are approximate.)

A good vacuum ($\approx 3 \times 10^{-5}$ Torr) is needed to produce a high-quality gold film and to avoid contamination of the spectra by outgassing and water vapor. A good test of the quality of the vacuum in the system is the strength of the 3200-cm^{-1} line from ice that generally grows with time in cold-finger cryostats below ≈ 150 K. This is the strongest line seen in the reflectance when ice develops on a metallic surface. In the initial stages of development, before the refinements mentioned above were introduced into the pumping system, at low temperatures (e.g., liquid nitrogen) ice was observed to form on the surface of the samples. By use of the optical constants of ice,[6] it was calculated that a film of water ice ≈ 100 nm thick formed after 2 h of exposure. After the improvements to the vacuum system were made, the ice line at 3200 cm^{-1} was no longer observed within this time frame.

The High-Tran unit is isolated from the interferometer vacuum by a sliding multiple-window holder, which may be translated under vacuum without loss of integrity. The window holder operates by using a combination of Viton O-rings and Teflon backup O-rings that sit in racetrack-shaped grooves. The window holder can accommodate two 25-mm-diameter windows: the first is 2-mil polypropylene (for measurements below 1000 cm^{-1}), and the second is KBr or KRS-5 (for measurements above ≈ 400 cm^{-1}). The window holder also has a third position, intermediate between the first two, which blanks off the system. Being able to blank off the system and then

replace the window is critical for the *in situ* evaporation technique. The radiation shield is held in place by a lock washer and has only two optical access ports to minimize the amount of room-temperature radiation absorbed by the sample or reference that might result in warming at low temperatures.

C. Evaporator

The evaporator plays a critical role in this system, and its design has been kept as simple as possible. Two electrical feedthroughs have been soldered onto a standard KF-25 stainless-steel blankoff. A brass post has been soldered to the center of the blankoff, and it terminates in a circular base that accommodates two stainless-steel posts that are soldered onto the electrical feedthroughs. The purpose of the central post is to relieve mechanical strain from the feedthroughs. The terminals are electrically isolated from the central supporting post by ceramic spacers. The filament consists of 0.125-μm-diameter tungsten wire, which has been coiled to form a filament (five or six turns to create a spiral ≈ 5 mm in length). The ends of the filament are attached to the stainless-steel terminals with screws and washers. The filament sits ≈ 1 cm from the front surface of the sample. For a gold evaporation ≈ 6 mm of 0.25-mm-diameter gold wire is cut into three lengths, and they are hung from the filament. A dc power supply passes current through the filament. A current of ≈ 3 A is applied for several seconds (until all the gold is evaporated). This produces a layer of gold of $\sim 3\delta$ (where δ is the classical skin depth) at 100 cm^{-1}, which ensures that multiple reflections do not occur. An indication that the gold evaporation has been successful is the formation of a gold surface on the viewing window, which fades to a bluish hue as the distance from the evaporator increases. The technique is similar for aluminum evaporations, except that different currents are required.

We determined the reflectance of gold films prepared at room temperature in this system by a multiple-bounce technique with a He–Ne laser. The measured reflectance agrees with the known values[2] to within 0.5%. In addition standards such as high-purity silicon were measured with both gold and aluminum films, and the reflectance was found to agree with the known values[2] to within 0.5%, confirming that the quality of the films is comparable with those of Ref. 2. Although the films adhere reliably to the sample, despite the attention to vacuum quality, they do not bond strongly. This may be partly because the gold or aluminum film is evaporated onto the sample at room temperature, whereas heating the substrate often produces films that are harder to remove. The fact that the films do not adhere firmly to the sample has the advantage that the gold film can be removed from the sample with tape, followed by a wash in methanol to remove any residue. This permits the sample to be used a number of times.

D. Procedure

We aligned the system initially by placing mirrors on the copper block attached to the bottom of the cold finger. A He–Ne laser brought in normal to the mirrors is used to adjust the mechanical stops until the rotation is exactly 90°. The mirrors are then removed and replaced by the cones. The sample (reference mirror) is attached to the tip of the cone with epoxy as shown in Fig. 4. We found that 5-min epoxy works well as a low-outgassing material that is able to withstand repeated thermal cycling. This epoxy is also soluble in hot acetone, which permits us to remove the sample and reuse it as well as the cone. Using the laser again, we adjusted the cones until the sample and the reference have roughly the same alignment. (This part of the procedure is not critical.) The cones are heat sunk to the copper block by three strands of copper braid, which are soldered to the back of the cones and pressed mechanically onto the copper block. Because of the geometry of the system, light that hits the sample is reflected back into the collecting toroid, but light that misses the sample is scattered out of the beam path. It is for this reason that the size of the aperture at the sample can be larger than the sample. This has the advantage not only of using the entire sample area but also of compensating for the thermal contraction of the tail of the refrigerator, which may shift by up to 1.0 mm in going from room temperature to 4.2 K. If a small aperture is used, the sample might shift out of focus, but because a larger spot is used the entire sample remains illuminated.

Once the system has been roughly aligned with the laser, the signal is optimized by adjusting the second $f/2.5$ toroidal mirror while keeping the scanning mirror stationary and using the vibrating-blade chopper placed in front of the aperture at the intermediate focus. Once the signal has been optimized, the mirror is not adjusted again.

When the sample and reference are rotated into the beam, interferograms are collected and co-added. The resulting power spectra are defined as those of the sample R_s and the reference R_r, but it is the ratio

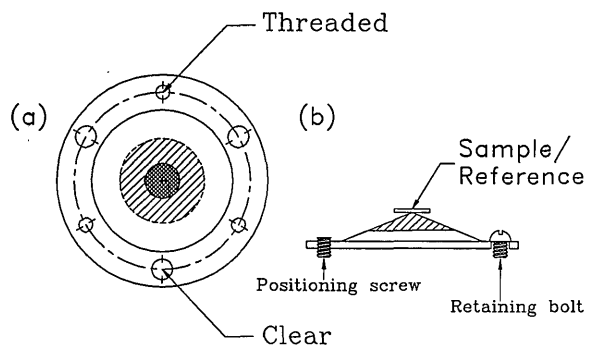

Fig. 4. Sample mounting arrangement: (a) The top view, showing the location of the mounting screws. The hatched lines indicate the usual size of the aperture on the cone, and the crosshatched area is the size of the sample. (b) The side view, showing the sample. The angle on the cones is typically $\geq 20°$.

of the two that is the important quantity, R_s/R_r. It is important to obtain this ratio for each temperature examined. After the data have been collected, the sample is rotated to face the evaporator and the window holder is moved to the blank position. When the evaporation is complete, the window is replaced and the data collection procedure is repeated at each temperature, resulting in a new set of power spectra for the gold (aluminum) evaporated sample R_{gs} and the pristine reference R_r. The effects of the reference mirror and any instrumental drift may be eliminated by taking

$$\left(\frac{R_s}{R_r}\right)\left(\frac{R_{gs}}{R_r}\right)^{-1} \equiv \frac{R_s}{R_{gs}}, \tag{1}$$

which is just the ratio of the reflectance of the sample with respect to gold (aluminum) at a given temperature. The reflectance may be obtained by taking the product with the known reflectance of gold (aluminum).[2]

3. Results

A. Background Test

Before any actual reflectance measurements could be made, a background test was performed to determine if a bare cone reflected any light back into the optical path.

A small stainless-steel mirror was mounted on one cone, while the other remained bare. Using the technique described above, we aligned the reference mirror, while the bare cone was simply bolted flat against the copper block. With the vacuum windows in place and using several different sources and detectors, we compared the power spectrum for the bare cone with that of the reference mirror. The ratio was zero, determined as accurately as the signal-to-noise ratio permitted ($\leq 0.5\%$), thus showing that the cones are optically black. It should be noted that this technique was also used to determine that window reflections were initially present. (These reflections have been removed by using the techniques described above.)

B. Thermometry

Because this system is designed for cryogenic applications, it is important to know the temperature of the sample at the tip of the cone. The temperature controller for the High-Tran uses a calibrated silicon diode located below the heat-exchanger element at the tip of the cold finger. However, it is reasonable to expect that the temperature at the tip of the cone will be higher than at the tip of the cold finger. To test the temperature gradient, we glued a small calibrated silicon diode to the tip of the cone; as the temperature was lowered from room temperature to ≈ 4.2 K, the temperature difference was compared. From room temperature down to ≈ 80 K, there is essentially no difference in the two temperatures. However, below ≈ 80 K the cone becomes several degrees warmer than the reading from the diode at the cold finger. As a result of several runs, at ≈ 4.2 K the temperature at the tip of the cone was $\approx 15 \pm 5$ K. We believe that this represents a conservative upper limit for the following reason: when compared with the sample, the diode, although only 1 mm × 2 mm × 1 mm in size, is larger and more bulky than a typical sample. We found that in many attempts a crack developed in the epoxy holding the element to the tip of the cone, possibly because of the strain imposed by the attached leads, which suggests a rather poor bond between the two. However, the samples are always quite firmly attached to the cone; often over an hour in hot acetone is required to remove them. The copper braid provides an important thermal link with the cold finger. Without it, even at ≈ 80 K the temperature is ≈ 15 K warmer at the tip of the cone than at the cold finger.

C. Reflectance of $SrTiO_3$

To test the method, we measured the reflectance of a single crystal of $SrTiO_3$ in two ways: first on a large polished surface of a single crystal and second on an irregular piece broken off the same sample. A scanning electron microscopy picture of the piece is shown in Fig. 5. Figure 6 shows the reflectance determined on the flat sample, solid curve, and the irregular piece, dashed curves, along with some data points from the literature.[7] The curve with the long dashes shows the signal from the irregular piece compared with a flat mirror, that is, before the gold correction has been applied. It can be seen that only a small fraction of the radiation that falls on the rough sample is actually collected by the optics. Nevertheless even with such a poor optical-quality surface, agreement with the polished surface is within 1%. The somewhat lower reflectance of the sample from Ref. 7 may be a result of intrinsic sample differences.

D. Quasi-crystal Reflectance

Another example of a difficult sample is the stable, icosahedral quasi-crystal $Al_{63.5}Cu_{24.5}Fe_{12}$. The material was originally prepared as a melt-spun ribbon,

Fig. 5. Irregular piece broken from a crystal of $SrTiO_3$ used to measure the spectra in Fig. 6.

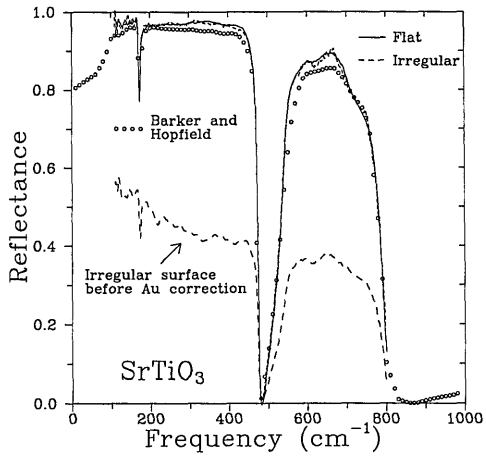

Fig. 6. Reflectance of $SrTiO_3$ measured on the irregular sample shown in Fig. 5, short-dashed curves; a large polished sample of the same material, solid curve; data from Barker and Hopfield,[7] circles. The curve with the long dashes shows the signal from the irregular sample referenced to a flat mirror.

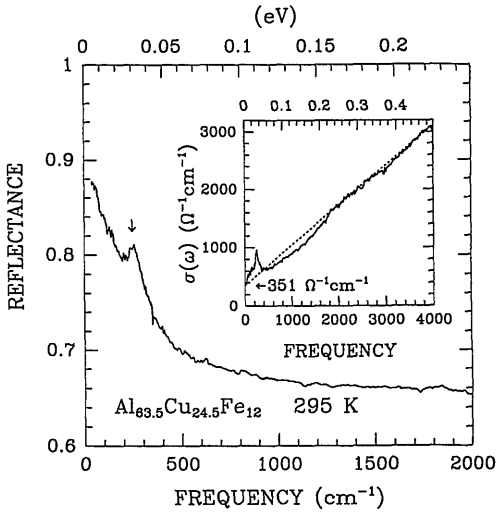

Fig. 7. Reflectance of $Al_{63.5}Cu_{24.5}Fe_{12}$ at 295 K from 30 to 2000 cm^{-1}. The inset shows the Kramers–Kronig optical conductivity over the same frequency range. The dashed line in the inset is the extrapolation of the conductivity to zero frequency. The value of the intercept is close to the measured dc conductivity for this material.

and it is subsequently annealed.[8] The result is an extremely thin, curved, brittle strip, silvery in visible light with an irregular surface. All attempts to polish these samples resulted in fracturing because of their glassy nature. A small piece of $Al_{63.5}Cu_{24.5}Fe_{12}$, $\approx 1 \times 1 \times 0.1$ mm was mounted on a cone in the manner described above. During the alignment with the He–Ne laser, it was observed that the reflected laser light was a diffuse cloud most intense in the center, at the expected position of the specularly reflected beam, but showing intensity out to large angles ($\geq 30°$). There were also bright spots within the field of scattered light, indicating that the nature of the surface irregularities varied considerably.

The ratios of the quasi-crystal and the coated quasi-crystal with respect to a polished stainless-steel reference mirror displayed a number of features in the far IR, whose origins were discussed in Section 1. When these two ratios were divided, these features disappeared leaving a smooth spectrum with a phonon feature at ≈ 240 cm^{-1}, as shown in Fig. 1. This result supports the argument that the effects in reflectance from surface scattering and filter absorptions caused by misalignments of the sample and reference are removed by the overcoating process.

The reflectance of $Al_{63.5}Cu_{24.5}Fe_{12}$ (corrected for the reflectance of gold, the overcoating material used in this frequency range) is shown at room temperature[8] in Fig. 7 from ≈ 30 to 2000 cm^{-1}. The noise in the reflectance over this region is less than $\approx 0.5\%$. The measurements have been extended to 25,000 cm^{-1} with a grating instrument, and the optical conductivity, shown in the inset in Fig. 7, has been calculated with the Kramers–Kronig analysis.[8] The extrapolated value for the dc conductivity (351 Ω^{-1} cm^{-1}) is in excellent agreement with the measured dc conductivity (357 Ω^{-1} cm^{-1}), which indicates that the optical result is consistent with transport measurements.[9] Alternatively this agreement could be taken as evidence that the overcoating method gives the correct value of the reflectance to better than 0.5%. Furthermore, there was good agreement (better than 1%) between overlapping regions, measured with different detectors and beam splitters.

4. Conclusions

Measuring the reflectance of small, irregular samples by using an *in situ* evaporation technique has been described. Comparison of the reflectance of $SrTiO_3$ measured on a polished flat with that of a sample of irregular shape and surface microstructure attests to the integrity of the method. Furthermore the reflectance of a novel material with an irregular surface geometry $Al_{63.5}Cu_{24.5}Fe_{12}$ has been measured. Structure that is introduced by surface scattering, and filter absorptions caused by misalignments of the sample and reference, is seen to be removed when the overcoating technique is used. For wavelengths comparable with the size of the sample, calculations performed on spheres show that the effects of diffraction may be reduced when the overcoating technique is used (see Appendix A). The measured results for $Al_{63.5}Cu_{24.5}Fe_{12}$ are found to be in good agreement with transport measurements made on this material. The overcoating technique corrects for a wide variety of geometries and permits the specular reflectance to be measured for an irregular surface. The optical properties may then be calculated by a Kramers–Kronig analysis.

Appendix A: Diffraction Effects

In any optical system, scattering caused by geometrical and diffraction effects will limit the efficiency of the system. In the case where the sample size is of the order of the wavelength, scattering resulting from microstructure usually becomes negligible and diffraction effects will be particularly important.[10]

With this technique the sample is coated with a layer of gold (or aluminum) so that the thickness is many times the skin depth over the frequency range of interest. If the sample being studied is a poor metal or an insulator, the change in the complex refractive index may be quite large. In the case of a flat surface where the reflectance is specular and the size of the sample is large (with respect to the wavelength), altering the refractive indices introduces no new complications and the problem is entirely geometrical. However, if the wavelength is of the order of the sample size, then, because of the presence of edges, the nature of the diffraction effects will depend on the refractive index of the material.

To demonstrate this effect, an example where analytical results are available is considered: the light scattered by a sphere. By using Mie theory,[11–13] it is possible to calculate exactly the angular efficiency of backscattering for a sphere with a complex refractive index. For details regarding the algorithms used to calculate this quantity, the reader is referred to Ref. 13, where this subject is examined in considerable detail.

To model the effects of overcoating a sphere, we consider a case where the complex refractive index of the sphere is modeled by using the Drude theory for metals. The Drude parameters for the uncoated sphere are taken to be $\omega_p = 1 \times 10^5\ \mathrm{cm}^{-1}$ and $\Gamma = 3 \times 10^5\ \mathrm{cm}^{-1}$, values that are consistent with a poor metal, yet still good enough that backscattering caused by internal reflections is eliminated (for spheres with a diameter of $\geq 100\ \mu\mathrm{m}$, a limit set by experimental considerations). The parameters for the coating material are similar to those of aluminum[2]: the plasma frequency is unaltered from the uncoated sphere, but the damping is much smaller, $\Gamma = 1 \times 10^4\ \mathrm{cm}^{-1}$, yielding a higher reflectance. The coating is assumed to be thick enough that it is many times the skin depth over the frequency range being studied.

In Fig. 8 a sphere of 0.5-mm radius and a detector with a 30° field of view (similar to the experimental values) are considered. The long-dashed curve is the reflectance of a specular surface when the Drude parameters of the uncoated material are used, and the dashed curve is the reflectance for the overcoating material; the dotted–dashed curve is the ratio of the two. The inset shows the value of the backscattering integral for a sphere (dashed curve) and the coated sphere (solid curve). The integral reveals a great deal of structure below $\approx 40\ \mathrm{cm}^{-1}$. The solid curve in the main figure is the result of dividing the integral for the sphere with that for the coated sphere. Above $\approx 40\ \mathrm{cm}^{-1}$ the result is the same to within 1% as the expected result from specular reflectance. Below 40 cm^{-1} the structure in the integral has not completely canceled out. However, the average value of the fringes agrees with the specular reflectance down to $\approx 5\ \mathrm{cm}^{-1}$, at which point it appears to become smaller than the expected result for specular reflectance. The residual fringes above 40 cm^{-1} may be reduced either by increasing the field of view or by making the sample larger.

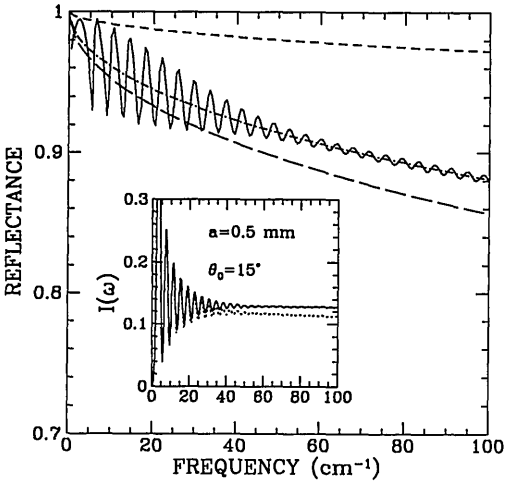

Fig. 8. Reflectance for a metal described by Drude theory with $\omega_p = 1 \times 10^5\ \mathrm{cm}^{-1}$, $\Gamma = 3 \times 10^5\ \mathrm{cm}^{-1}$ (long-dashed curve), and the reflectance for a metal with the same ω_p but with a much smaller damping, $\Gamma = 1 \times 10^4\ \mathrm{cm}^{-1}$ (dashed curve), $\epsilon_\infty = 1$ in both cases. The dot–dashed curve is the ratio of the first with respect to the second. The inset shows the value of the backscatter efficiency $I(\omega)$ for a sphere with a 1.0-μm diameter for the first set of Drude parameters (dotted curve) and the coated sphere (solid curve). The detector field of view is 30°. The solid curve in the main diagram is the ratio of the two curves in the inset. Above $\approx 40\ \mathrm{cm}^{-1}$ the reflectance calculated for spheres agrees with the result for specular reflectance to within 1%.

These calculations show that the backscattered intensity ratio gives a good approximation of the specular reflectance, a result that is consistent with the experimental results. However, this calculation is for a sphere and thus only a single source of diffraction; in samples with more complicated geometries the diffraction will be altered, but by extension the ratio should still give the specular reflectance.

We acknowledge the useful suggestions and technical expertise of C. Berwick, M. Roberts, and G. Innocente during the many different stages of this project. We also acknowledge assistance from B. Zvan and A. Duncan in the laboratory. The scanninig electronc microscope photograph was taken by J. Hudak. This study was supported by the Natural Sciences and Engineering Research Council of Canada and the Canadian Institute for Advanced Research.

References

1. F. Wooten, *Optical Properties of Solids* (Academic, New York, 1972), pp. 173–182.
2. D. W. Lynch and W. R. Hunter, "Comments on the optical constants of metals and an introduction to the data for several metals," in *Handbook of Optical Constants of Solids*, E. D. Palik, ed. (Academic, New York, 1985), pp. 286–295; D. Y. Smith, E. Shiles, and M. Inokuti, "Optical properties of metallic aluminum," in *Handbook of Optical Constants of Solids*, E. D. Palik, ed. (Academic, New York, 1985), pp. 369–383.
3. C. S. Jacobsen, D. B. Tanner, and K. Bechgaard, "Optical

and infrared properties of tetramethyltetraselenafulvalene [$(TMTSF)_2X$] and tetramethyltetrathiafulvalene [$(TMTTF)_2X$] compounds," Phys. Rev. B **28,** 7019–7032 (1983).
4. R. T. Collins, Z. Schlesinger, F. Holtzberg, and C. Field, "Infrared evidence for gap anisotropy in $YBa_2Cu_3O_7$," Phys. Rev. Lett. **63,** 422–425 (1989).
5. J. E. Eldridge and C. C. Homes, "Low-temperature, small-sample reflectivity measurements in a commercial rapid-scan Michelson interferometer," Infrared Phys. **29,** 143–148 (1989).
6. J. E. Bertie, J. J. Labbé, and E. Whalley, "Absorptivity of ice I in the range 4000–30 cm^{-1}," J. Chem. Phys. **50,** 4501–4516 (1969).
7. A. S. Barker and J. J. Hopfield, "Coupled-optical-phonon-mode theory of the infrared dispersion in $BaTiO_3$, $SrTiO_3$, and $KTaO_3$," Phys. Rev. A **135,** 1735, (1964), cited by F. Gervais, "Strontium titanate ($SrTiO_3$)," in *Handbook of Optical Constants of Solids II,* E. D. Palik, ed. (Academic, New York, 1991), pp. 1035–1047.
8. C. C. Homes, T. Timusk, X. Wu, Z. Altounian, A. Sahnoune, and J. O. Ström-Olsen, "Optical conductivity of the stable icosahedral quasicrystal $Al_{63.5}Cu_{24.5}Fe_{12}$," Phys. Rev. Lett. **67,** 2694–2696 (1991).
9. B. D. Biggs, Y. Li, and S. J. Poon, "Electronic properties of icosahedral, approximant and amorphous phases of an Al–Cu–Fe alloy," Phys. Rev. B **43,** 8747–8750 (1991).
10. C. C. Homes, "Optical properties of $(TMTSF)_2ReO_4$ and $(TMTSF)_2BF_4$ above and below their metal–insulator transitions," Ph.D. dissertation (University of British Columbia, Vancouver, B.C. V6T 2A6, Canada, 1990), pp. 45–49.
11. G. Mie, "Beitrage zur Optik trüber Medien speziell kollaidaler Metallösungen," Ann. Phys. **25,** 377–445 (1908).
12. H. C. van de Hulst, *Light Scattering by Small Particles* (Wiley, New York, 1957).
13. C. F. Bohren and D. R. Huffman, "Absorption and scattering by a sphere," in *Scattering of Light by Small Particles* (Wiley, New York, 1983), pp. 120–123.